Arab J Sci Eng (2018) 43:1839–1863
https://doi.org/10.1007/s13369-017-2771-0

RESEARCH ARTICLE - CIVIL ENGINEERING

Static and Dynamic Structural Performances of a Special-Shaped Concrete-Filled Steel Tubular Arch Bridge in Extreme Events Using a Validated Computational Model

X. X. Cheng[1] · J. Dong[1] · S. S. Cao[2] · X. L. Han[3] · C. Q. Miao[3]

Received: 4 January 2017 / Accepted: 1 August 2017 / Published online: 20 August 2017

Abstract Recently, Yingzhou Bridge with a main span of 120 m has been built in Luoyang, China. Although the bridge's unique concrete-filled steel tubular arch-rib system satisfies the aesthetic demand of the public, the innovative structure's mechanics behaviors in extreme events are unknown yet, including both static and dynamic structural performances. To this end, numerical analyses have been undertaken based on ANSYS finite-element (FE) platform (version 9.0). A simplified computational FE model is established and effectively updated using reference information obtained from a detailed FE model. Using the validated simplified FE model, the bridge's stability, ultimate load-carrying capacity and seismic performance are studied considering the original design and several modified designs. It is found that the bridge's performances basically meet the design requirements; however, the structure's lateral stability and stiffness are relatively weak for the original design. Adding K-shaped struts and reducing subarches' angle of inclination can effectively solve this problem.

Keywords Special-shaped arch bridge · Finite-element model · Model updating · Stability · Ultimate load-carrying capacity · Seismic performance

✉ J. Dong
dongjun@njtech.edu.cn

[1] College of Civil Engineering, Nanjing Tech University, Nanjing 211816, China

[2] School of Civil Engineering, Guangzhou University, Guangzhou 510006, China

[3] School of Civil Engineering, Southeast University, Nanjing 210096, China

1 Introduction

As China stages its fast development in urban transportation, higher expectations are given for the aesthetic value of bridges under construction. A type of special-shaped spatial arch-rib system have been designed for some arch bridges in China, such as Longjiang Bridge in Zhangzhou (see Fig. 1a), Donggang Bridge in Changzhou (see Fig. 1b), Jiubao Bridge in Hangzhou (see Fig. 1c), Changfeng Bridge in Ningbo (see Fig. 1d), Yitong River Bridge in Changchun (see Fig. 1e) and Yingzhou Bridge in Luoyang (see Fig. 1f) [1]. The system is a reversed triangular cross-sectioned structure comprising three arch-ribs (one main arch in the middle and two subarches at two sides) intersecting at two skewbacks and connected by lateral and inclined struts above (see Fig. 2), which is literally known as "moon-arch" owing to the system's moon-shaped appearance. Though its unique appearance satisfies the aesthetic demands of general public, this innovative structure's mechanical behaviors in extreme events have not been completely understood yet. Comparing the new structure to the traditional tie arch bridges with vertical parallel arches, it can be found that the lateral span between subarches is large and the number of lateral connection members between arches is small. Whether these might adversely affect the structural performances is worth investigating. If they do, we need to further find out to what extent the innovative structural form influences its mechanical behaviors and what improvements can be adopted.

Generally, physical experiments are not possible for the above-mentioned researches, and the numerical simulation is an effective approach. Today, almost all extreme events experienced by structures can be numerically simulated using commercially available FE programs, including the excessive loading and the earthquake. However, the accuracy

Fig. 1 View of special-shaped arch bridges. **a** Longjiang Bridge. **b** Donggang Bridge. **c** Jiubao Bridge. **d** Changfeng Bridge. **e** Yitong River Bridge. **f** Yingzhou Bridge

of numerical analyses deserves our attention. An important issue is the similarity problem with the FE model, as the computational models we employ are generally simplified models with some assumptions which might be different from the physical truth. In this regard, these models should be validated before being used. For inaccurate models, model updating is required. According to Zhang et al. [2], the effects of model updating are significant on the structural responses for this type of structures.

Model updating can basically be regarded as an optimization process, during which the model's dynamic and static characteristics gradually get closer to the reference information through changes in uncertain parameters. The reference information is usually modal parameters measured on the full-scale structures. However, the measured dynamic characteristics for model updating might be uncertain as they usually vary in intervals. Some researchers attribute this uncertainty to the differences of techniques used to determine the dynamic characteristics of structures and conduct related researches. Fei et al. [3] employ two modal identification methods to identify the modal frequencies of both Runyang suspension and Runyang cable-stayed bridges from data measured by accelerometers installed on main girders of the bridges, i.e., the enhanced frequency domain decomposition (EFDD) and the stochastic subspace identification

(SSI). The maximum relative difference of results between the two techniques is 0.49% for the cable-stayed bridge, and it is 0.54% for the suspension bridge. Bayraktar et al. [4] use two methods, i.e., peak picking (PP) and SSI, to attain dynamic characteristic of Senyuva historic arch bridge experimentally. The maximum relative difference of experimental frequency between the two methods appears in the fifth mode, reaching 3.37%. Bayraktar et al. [5] also use EFDD and SSI to determine the natural frequencies of a reinforced concrete minaret. The maximum relative difference between the results using the two methods is 6.1%, while the maximum relative difference of natural frequencies between two tests using the same modal identification method (i.e. EFDD) can reach 7.9%. It seems to indicate that the difference of the modal identification technique causes some uncertainties to measured experimental frequencies; however, other more significant influences also exist. According to some other researches, temperature can also affect structural dynamic characteristics. Abdel Wahab and De Roeck [6] have conducted two dynamic tests for a prestressed concrete bridge in spring and winter, respectively, and have found an increase of 4–5% in modal frequencies with the decrease in temperature. Cornwell et al. [7] have observed the variability of modal frequencies by up to 6% over a 24-h period on the Alamosa Canyon Bridge. Ding and Li [8] have studied the temperature-induced variations of measured modal frequencies of the steel box girder of a suspension bridge using long-term monitoring data. Decreases of 2.2–2.9% in modal frequencies were observed with the increase in temperature for all the identified modes using 10-min data segments. Teng et al. [9] have measured the modal frequencies of a large steel structure and have found that the relative differences of results are 1.8–4.2% for different tests. Although Teng et al. attributed the differences to the measurement noise and signal processing errors, the effect of temperature on the dynamic frequencies should not be disregarded. In view of the above, 5% difference of measured modal frequencies caused by the temperature change is common for large civil structures, so occasionally field modal tests can hardly provide reference information of high certainty for model updating. To deal with this problem, it is proposed in this paper to obtain reliable reference information from detailed FE models. Since detailed models truly simulate all the details of the structures, the spatial distributions of mass and stiffness are highly accurate for them. Thus, dependable structural dynamic characteristics can be produced using detailed models, which is proved by Brownjohn and Xia [10] and Kilic et al. [11].

In view of this narrative, this paper employs the special-shaped Yingzhou Bridge located in Luoyang, China, as the engineering background. The bridge is modeled in a simple way for computational efficiency. Then, model updating is undertaken for the simplified model using reference information from a detailed model. Using the updated model, Yingzhou Bridge's structural stability, ultimate load-carrying capacity and seismic performance are studied. The numerical analyses are reliable since the updated model has been validated using field static load test results, and the findings of numerical analyses are of practical significance.

2 Numerical Modeling of Yingzhou Bridge

2.1 Yingzhou Bridge's Structural Design

Yingzhou Bridge is a half-through tied arch bridge with a span of 120 m. As is shown in Fig. 2, its special-shaped arch-rib system of reversed triangular cross section comprises one concrete-filled steel tubular arch in the middle and two hollow

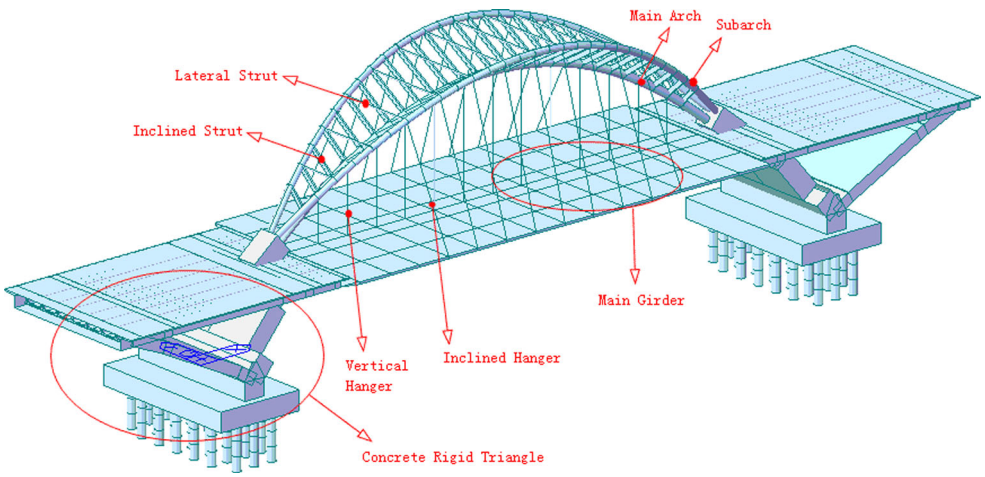

Fig. 2 Structural components of Yingzhou Bridge

steel tubular subarches at two sides. They intersect at skewbacks and are connected by lateral and inclined steel struts above. The steel hangers are uniformly attached to the three arches to form one vertical hanger plane and two inclined hanger planes. Suspended by hangers, the main deck is a steel-concrete composite box girder with prestressed cable ties inside. At skewbacks, two huge concrete rigid triangles are designed which comprise caps, arch-ribs and piers. The cross section and the material properties for the main structural components of the bridge are listed in Table 1.

Although it is a complicated spatial structure, the designers clearly show the bridge's load-transferring path using Fig. 3. The whole structure can be divided into two load-carrying systems. The first system is composed of the arch-rib system, the two concrete rigid triangles and the prestressed cable ties. It looks like a bow, which carries the loads from the hangers. The second system is composed of hangers and the main deck, which mainly carries the vehicle loads.

2.2 FE Models

First, a detailed FE model is established on ANSYS platform (version 9.0) (see Fig. 4a). The arch-rib system is modeled by beam elements. When simulating the concrete-filled steel tubular arch (the main arch), the material constitutive model is obtained based on converted material method, which is widely used in many countries' Codes of Practice. The hangers are modeled by bar elements, and the two concrete rigid triangles are modeled by solid elements. Moreover, all the details of the steel box girder are modeled using shell elements. An advanced MPC technique (see Ref. [27] for details) is employed to assemble different components to form the entire bridge.

Second, a simplified FE model is established on ANSYS platform by using beam or bar elements of equivalent cross sections to simulate all structural components (see Fig. 4b). The whole box girder is modeled using one beam. The bending, torsional and inertial properties of the realistic box girder are simulated by adjusting the beam's elastic modulus, density and moments of inertia. The concrete rigid triangles and the arch-rib system are also simulated using beam elements. For computational efficiency, the simplified FE model will be used as the computational model for following numerical analyses, and the detailed model will be used to validate the accuracy of the simplified model.

Modal analyses are preformed for both the simplified FE model and the detailed FE model, and the results are shown in Fig. 5. Comparison of results made in Table 2 suggests that the simplified model is basically qualified, since the root-mean-square value (RMS) of all modal frequency relative differences is 5.16%. However, the relative modal frequency differences between the two models are

Table 1 Cross section and material properties for main structural components

Structural component	Section type	Area (m^2)	In-plane moment of inertia (m^4)	Out-of-plane moment of inertia (m^4)	Torsional moment of inertia (m^4)
Main arch	Circular solid	1.767	0.249	0.249	0.497
Subarch	Circular tube	0.081	0.014	0.014	0.028
Lateral strut	Circular tube	0.025	0.0002	0.0002	0.0005
Inclined strut	I-shaped section	0.024	0.0023	0.00005	–
Main girder	Box section	1.072	75.953	45.83	27.33
Concrete rigid triangle-A	Rectangle	57.2	23.07	322.2	–
Concrete rigid triangle-B	Rectangle	63	64.3	170.1	–
Concrete rigid triangle-C	Rectangle	52	17.3	292.9	–

Material	E (GPa)	ρ (kg/m^3)	γ	σ_y (MPa)
Concrete-filled steel tube	43.37	2770	0.1677	55.63
Steel	206	7850	0.25	345
Concrete	34.5	2500	0.17	32.4
Hangers and cables	206	8400	0.3	–

E elastic modulus, γ Poisson's ratio, σ_y yield stress of material, ρ weight per unit volume of material

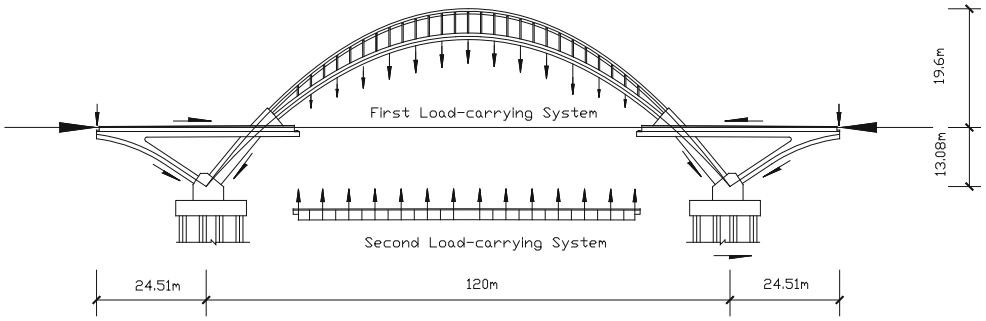

Fig. 3 Load-transferring path

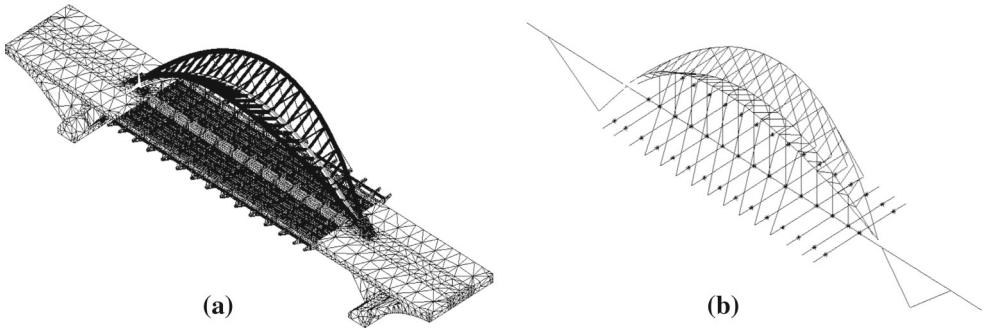

Fig. 4 FE models established on ANSYS platform. **a** Detailed FE model. **b** Simplified FE model

large for a few modes, e.g., the difference for the 5th mode is greater than 10%. So model updating should be undertaken to improve the accuracy of the simplified model.

The modal frequencies obtained in this paper are compared with FE analysis and full-scale measurement results from other literatures, as well as those obtained on another FE platform. Ref. [16] also establishes Yingzhou Bridge's FE model on ANSYS platform in a simple way employing one plate of shell elements to simulate the whole main girder. As can be seen in Table 2, the RMS of relative differences between modal frequencies obtained using our detailed model and those reported in Ref. [16] is 28.72%. For lateral and vertical bending modes, the relative differences are kept within 20%. However, they are greater than 40% for the two torsional modes, indicating that the practice of simulating the whole main girder using a plate of shell elements adopted by Ref. [16] causes significant underestimation of the torsional stiffness of the main girder. Besides, comparing our FE results to the field measurement results reported in Ref. [13], it is found in Table 2 that the discrepancies are huge, as the RMS of relative differences is 45.51%. We do not speak that experimental data inevitably contain a certain level of measurement noise [17]. The issues proposed for the reliability of ambient modal tests in Sect. 1 can hardly be solved, which probably cause the huge discrepancies between our FE results and the field measurement results. Furthermore, results for our detailed model established on ANSYS platform are also compared with those for another FE model established on MIDAS platform whose modeling strategy basically follows that of the simplified ANSYS model in Table 2. Modes obtained by using the MIDAS model are shown in Fig. 6. It is widely acknowledged that ANSYS is a research-oriented FE platform, while MIDAS is more design-oriented. However, the comparatively good agreement between the results obtained from the two models established on different platforms suggests that the difference in the structural analysis program used does not have a significant influence on the analysis results. Based on the basic theories of FE method, the assumptions and limitations for different commercially available FE programs should be the same.

3 Model Updating and Validation

In this portion of the study, the simplified computational FE model is updated based on the theories presented by Jaishi and Ren [12]. First, the sensitivity analysis is conducted to determine the significant parameters for model updating. Second, optimization is conducted by adjusting the values of those significant parameters to obtain a model whose dynamic characteristics accord with the reference information obtained from the detailed model. Third, the accuracy of the updated computational FE model is validated using field static load test results

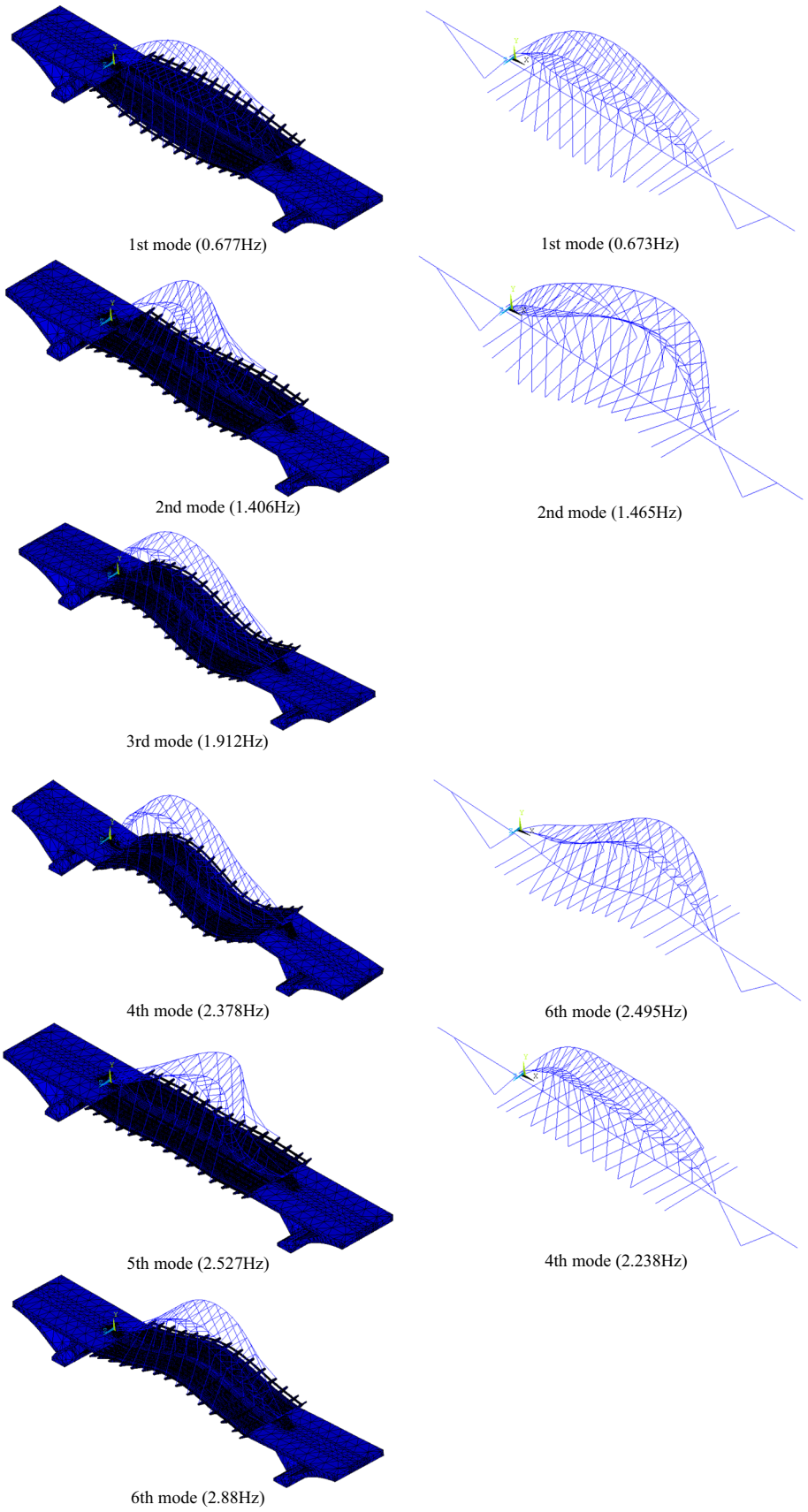

Fig. 5 Analytical modes obtained using the two FE models established on ANSYS platform. **a** Detailed FE model. **b** Simplified FE model

Fig. 5 continued

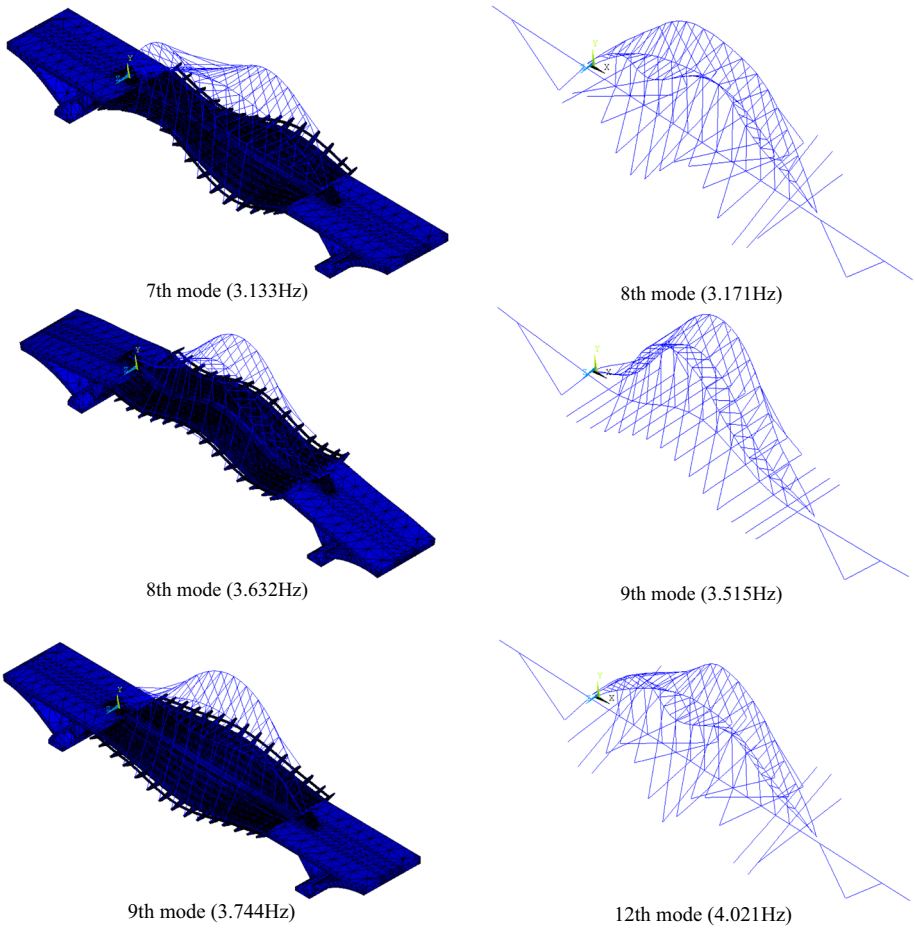

(a) Detailed FE model **(b)** Simplified FE model

3.1 Parameter Selection for Model Updating

All important design parameters are considered as variables in sensitivity analysis, including the density and the elastic modulus of the main girder, those of the main arch, those of the subarches, those of the transverse struts between arches, vertical and inclined hangers' elastic modulus and concrete's elastic modulus and density for the rigid triangle zones. The lower and upper limits for all variables are set as 0.9 and 1.1 times the design value, respectively. Based on the theory presented by Jaishi and Ren [12], sensitivity analyses are conducted on the simplified FE model, and the results are shown in Fig. 7.

It can be seen from Fig. 7 that all modal frequencies are sensitive to some design parameters, including the main girder's density and elastic modulus, the main arch's density and the struts' elastic modulus (Parameter Group 1). Besides, a few modal frequencies are sensitive to some other design parameters, including the main arch's elastic modulus, the vertical hangers' and inclined hangers' elastic modulus, and concrete's elastic modulus and density (Parameter Group 2). For the effectiveness of model updating, all parameters in Parameter Group 1 and Parameter Group 2 are selected as updated parameters.

3.2 Model Updating Based on Optimization Technique

Using subproblem optimization technique (see Ref. [12]), model updating is conducted on the simplified FE model. For the realness of the updated parameters, the constraints for all updated parameters are set to be $\pm 20\%$. The constrained objective function is the RMS of the relative differences between the low-order modal frequencies of the simplified model and those of the detailed model. The state variables are the low-order modal frequencies whose lower/upper bounds are $\pm 20\%$. The model updating using subproblem optimization technique is basically to minimize the penalty function-based unconstrained objective function through iterations. After many iterations, the optimized parameters are finally obtained within the allowable bounds (see Table 3), and the results of model updating are presented in Table 4. As shown, the differences of all modal frequencies for the updated model are below 3%, and the RMS of relative differences is 1.57% after model updating.

Table 2 Modal analysis results for FE analyses and full-scale measurements

Detailed FE model established on ANSYS platform			Simplified FE model established on ANSYS platform		
Mode no.	Modal frequency (Hz)	Mode shape*	Mode no.	Modal frequency (Hz)	Difference (%)
1	0.677	Arch's symmetrical lateral bending + deck's torsion	1	0.673	−0.59
2	1.406	Arch's antisymmetric lateral bending + deck's torsion	2	1.465	4.20
3	1.912	Arch's and deck's antisymmetric vertical bending	–	–	–
4	2.378	Whole bridge's antisymmetric vertical bending	6	2.495	4.92
5	2.527	Arch's symmetrical lateral bending	4	2.238	−11.44
6	2.88	Arch's and deck's symmetrical vertical bending	–	–	–
7	3.133	Arch's and deck's antisymmetric torsion	8	3.171	1.21
8	3.632	Whole bridge's symmetrical vertical bending	9	3.515	−3.22
9	3.744	Arch's and deck's symmetrical torsion	12	4.021	7.40
			RMS		**5.85**

FE model from Ref. [16]			Full-scale measurements according to Ref. [13]			FE model established on MIDAS platform		
Mode no.	Modal frequency (Hz)	Difference (%)	Mode no.	Modal frequency (Hz)	Difference (%)	Mode no.	Modal frequency (Hz)	Difference (%)
1	0.562	16.99	1	1.25	84.64	1	0.68	0.44
2	1.497	6.47	–	–	–	2	1.334	5.12
3	1.541	19.40	2	2	4.60	3	1.558	18.51
–	–	–	–	–	–	4	2.287	3.83
–	–	–	–	–	–	–	–	–
8	2.835	1.56	–	–	–	5	2.723	5.45
4	1.584	49.44	4	3.875	23.68	6	3.129	0.13
–	–	–	–	–	–	9	3.869	6.53
5	2.158	42.36	3	2.875	23.21	10	4.419	18.03
RMS		**28.72**	**RMS**		**45.51**	**RMS**		**9.88**

* The whole bridge refers to the arch-rib system, the concrete rigid triangles and the box girder as a whole

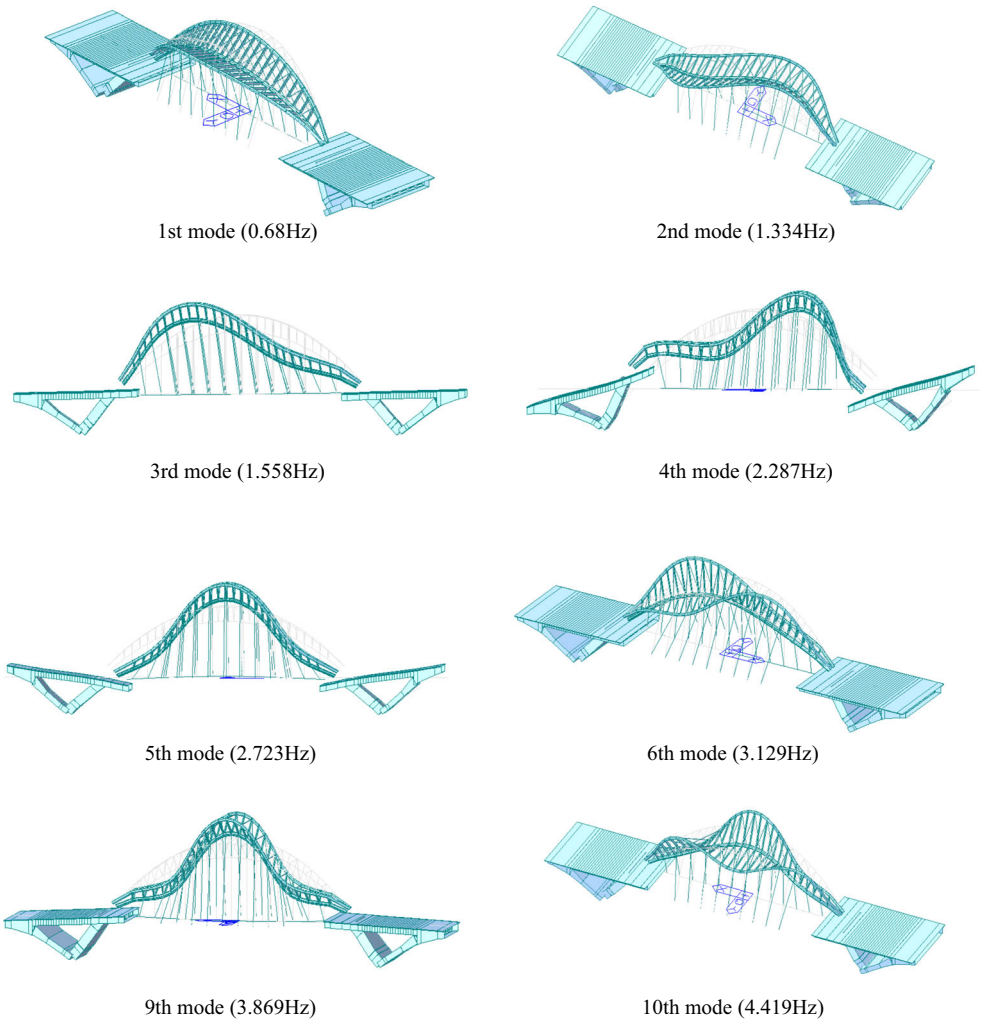

Fig. 6 Analytical modes obtained using the FE model established on MIDAS platform

3.3 Validating the Updated Model Using Static Load Test Results

To validate the quality of the updated model, field static load test results reported by Wu [13] are employed. The test is conducted on Yingzhou Bridge before it is open to traffic in 2009. As shown in Fig. 8a–f, six static load test cases are set to evaluate the static behavior of the bridge. Four to twelve 300-kN trucks are used for different cases. Fourteen vertical displacement measurement points are arranged on the deck (see Fig. 8g).

Using the simplified computational model with and without model updating, the six static load test cases are simulated, respectively. Comparisons between calculated and measured results made in Fig. 9 suggest that the calculated vertical displacements for the computational model without model updating are notably different from the measured results for all cases. However, after the model is updated, the numerical results are much closer to the measured results for almost all cases. The good agreement of structural responses is a supportive evidence of the quality of model updating. Up to this point, a validated computational FE model is obtained for following studies.

3.4 Validating the Detailed Model Using Static Load Test Results

Since the validity of the simplified model depends primarily on the validity of the detailed model, whether or not the detailed model itself is adequately representative of the real structure is of absolute significance. In this regard, the performance of the detailed model in predicting the results of the field static load test is studied in this portion of study. The results of numerical simulation of static load test case 1 using the detailed model are presented in Fig. 10. As can

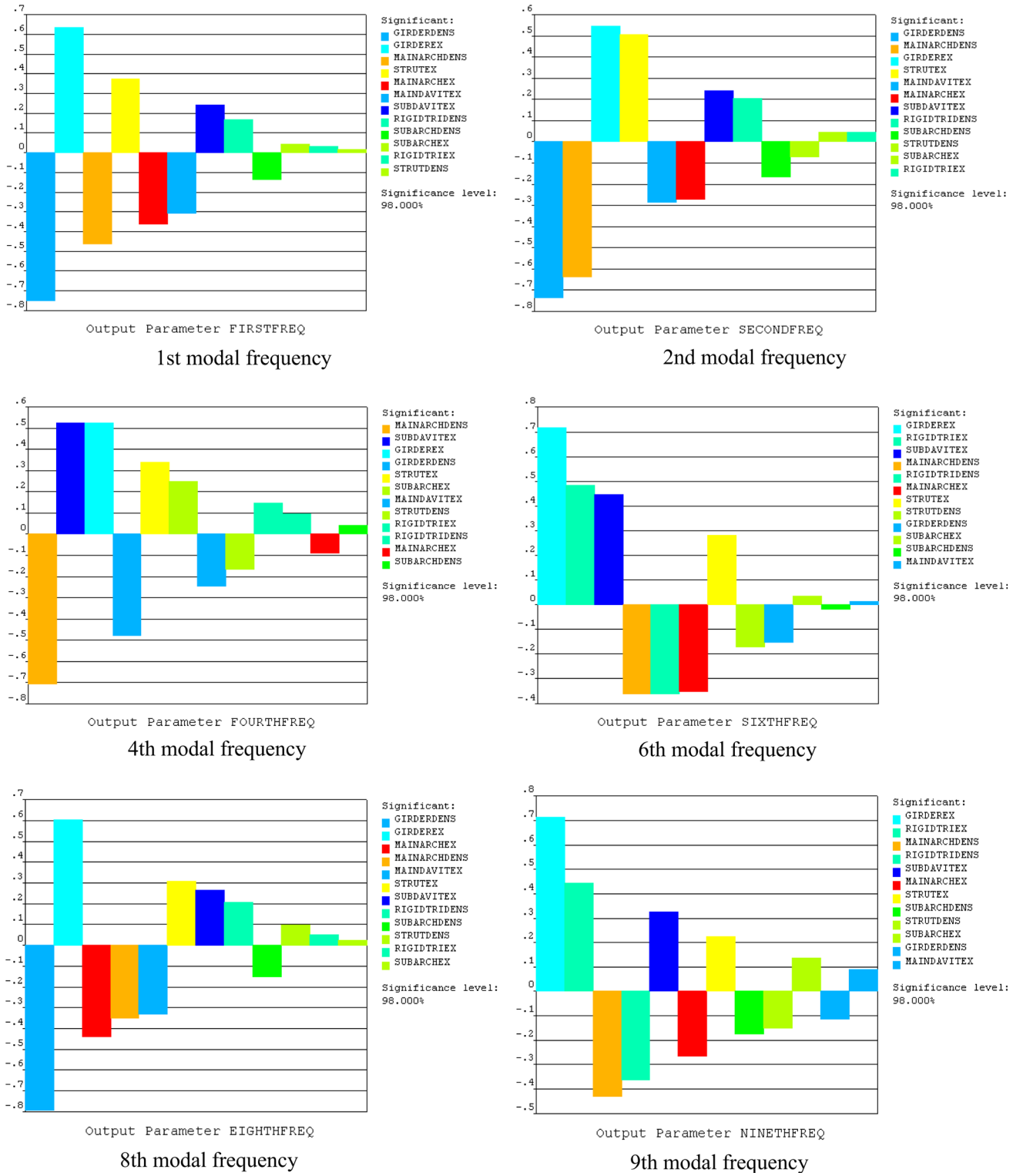

Fig. 7 Sensitivities of modal frequencies to design parameters. *Note* GIRDERDENS—main girder's density; GIRDEREX—main girder's elastic modulus; MAINARCHDENS—main arch's density; MAINARCHEX—main arch's elastic modulus; STRUTEX—struts' elastic modulus; STRUTDENS—struts' density; RIGIDTRIEX—concrete's elastic modulus; RIGIDTRIDENS—concrete's density; MAINDAVITEX—vertical hangers' elastic modulus; SUBDAVITEX—inclined hangers' elastic modulus; SUBARCHDENS—subarches' density; SUBARCHEX—subarches' elastic modulus

Table 3 Values of updated parameters before/after updating

Updated parameters	Main arch-rib		Main girder		Concrete in rigid Triangle zone		Main hanger's elastic modulus (e11 Pa)	Inclined hanger's elastic modulus (e11 Pa)	Strut's elastic modulus (e11 Pa)
	Density (kg/m^3)	Elastic modulus (e10 Pa)	Density (kg/m^3)	Elastic modulus (e11 Pa)	Density (kg/m^3)	Elastic modulus (e10 Pa)			
Before updating	2770	4.337	7850	2.06	2500	3.45	2.06	2.06	2.06
After updating	2222.1	4.307	7872.1	2.022	2877.8	3.466	1.664	2.122	1.658
Relative changes	19.8%	0.69%	0.28%	1.8%	15.1%	0.46%	19.2%	3.0%	19.5%

be seen, the calculated displacements along the bridge and the calculated along-bridge stresses at midspan cross section of the box girder agree well with the measured results reported in Ref. [13] (see Fig. 10b, c, respectively). The validity of the detailed model is therefore proved. Besides, the stress responses on every detail of the bridge are predicted in Fig. 10a, demonstrating usefulness of the detailed model. Unfortunately, the simple static analyses are all the detailed model can be used to do at present. When the detailed model is employed to conduct the linear elastic structural stability analysis, the calculated low order instability shapes are all local buckling patterns, which are of no practical significance. Besides, since the detailed model consists of 85238 elements, it is impossible to conduct advanced static and dynamic analyses due to the high computational cost. We tried many times to perform the ultimate load-carrying capacity analysis and the seismic analysis using the detailed model on an usual personal computer that has a 2.5 GHz CPU and a 3 GB memory, but it doesn't work out okay. The computational process takes a long time everytime, and the program always stops without a solution. As it now stands, it appears that the computing power is a critical issue in utilizing the detailed model, so the simplified model will be employed for the following analyses.

4 Static Performance

In this portion of the study, Yingzhou bridge's static performances under excessive loadings are studied using the simplified computational model, including its linear elastic stabilities and its ultimate load-carrying capacities. The former are based on bifurcation theory, and the latter are based on ultimate state theory.

4.1 Structural Stability

4.1.1 Structural Stability for the Original Structure

The linear elastic structural stability analysis is basically an eigenvalue problem. Since it is comparatively simple and of practical significance in indicating the structure's safety margin, linear elastic structural stability analysis has been widely used in structural design. In this paper, eight load cases are considered for linear elastic structural stability analysis according to Ministry of Transport, P.R.C. [14]:

Load Case 1: Dead load;
Load Case 2: Dead load + wind load;
Load Case 3: Dead load + pedestrian load;
Load Case 4: Dead load + full-bridge full-way lane load;
Load Case 5: Dead load + full-bridge half-way lane load;
Load Case 6: Dead load + half-bridge full-way lane load;

Table 4 Modal analyses results for the simplified FE model before/after model updating

Detailed FE model		Simplified FE model				
		Before model updating			After model updating	
Mode no.	Modal frequency (Hz)	Mode no.	Modal frequency (Hz)	Difference (%)	Modal frequency (Hz)	Difference (%)
1	0.677	1	0.673	−0.59	0.679	0.30
2	1.406	2	1.465	4.20	1.433	1.92
3	1.912	–	–	–	–	–
4	2.378	6	2.495	4.92	2.349	−1.22
5	2.527	4	2.238	−11.44	2.489	−1.50
6	2.88	–	–	–	–	–
7	3.133	8	3.171	1.21	3.142	0.29
8	3.632	9	3.515	−3.22	3.527	−2.89
9	3.744	12	4.021	7.40	3.786	1.12
RMS				**5.85**		**1.57**

Load Case 7: Dead load + full-bridge full-way lane load + pedestrian load;
Load Case 8: Dead load + wind load + full-bridge full-way lane load + pedestrian load.

Using the updated computational model, Yingzhou Bridge's stabilities for all eight load cases are calculated. Results listed in Table 5 suggest that the eigenvalues obtained for Cases 1–6 are larger than those for Cases 7 and 8. This is because Cases 1–6 consider fewer loads comparing to Cases 7 and 8. Cases 7 and 8 comprehensively take all kinds of loads into account, for which eigenvalues are of practical significance. Besides, it can be found by comparing Cases 1–4 that the effects of the lane load on the structural stability are more notable than those of wind load and pedestrian load. Comparing Cases 4–6, it can be found that it is a conservative practice to consider full-bridge full-way lane load, and the case of half-bridge lane load is more unfavorable than the case of half-way lane load with respect to the structural stability. On the whole, the stability eigenvalues for all load cases meet the design requirements.

But stability analyses also suggest that the bridge is of poor out-plane (lateral) stability. From Table 5, the lowest order in-plane eigenvalues are much greater than the lowest order out-plane eigenvalues for all load cases. The low-order instability shapes for Load Case 1 are shown in Fig. 11. As can be seen, all of the first five lowest order instability shapes are the out-plane patterns, and the in-plane instability shape occurs at the sixth order. Same situation holds true for other load cases. To this end, the original design deserves to be improved to enhance the structure's lateral stability.

To improve the bridge's lateral stability, six usual countermeasures are proposed in the following subsections, including adding horizontal struts, using new types of struts, increasing the stiffness of struts, changing inclination angle of subarches, increasing stiffness of inclined hangers and increasing the torsional stiffness of the box girder. These countermeasures do not markedly change the original design, and most of them are easy to implement.

4.1.2 Structural Stability for the Structure with Added Horizontal Struts

In the special-shaped arch-rib system, the horizontal struts connect the two subarches horizontally. Thirteen struts are set for the original design, whose neighboring spacing is 6 m. The modified structure has 25 struts, whose neighboring spacing is 3 m (see Fig. 12).

Using Load Case 7, the stability analyses are preformed for original structure and the modified structure, respectively. The results listed in Table 6 suggest that the strut number has little effects on the in-plane (6th order) structural stability, but it has some effects on out-plane (first four lowest order) structural stability. When the strut number is doubled, the first four lowest order stability eigenvalues increase by 6.98, 7.78, 4.33 and 3.39%, respectively.

4.1.3 Structural Stability for the Structure with New Types of Struts

When out-plane instability occurs, the struts at the vault stand the torsional forces acting on the arches. It has been proved that perpendicularly arranged struts can effectively reduce the arches' torsion there. However, struts located in 1/4 midspans stand the relative displacement between arches. If the struts are arranged tangentially there (e.g., using K-shaped struts), the displacement controlling effects are found to be better. In this regard, four new types of struts (Cases 1–4) are, respectively, added to the original structure in between the two subarches, as shown in Fig. 13.

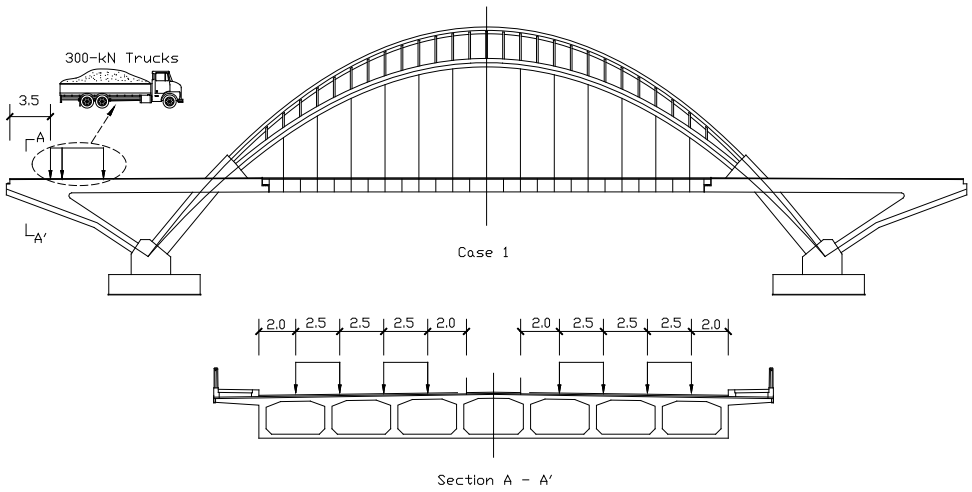

(a)

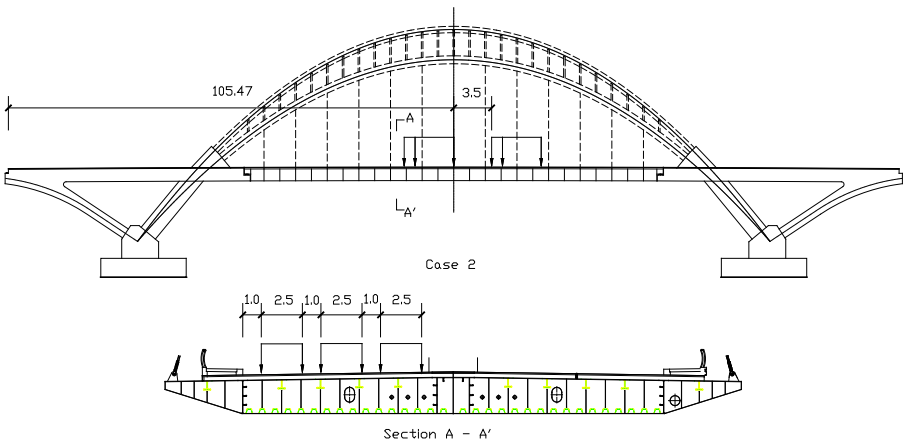

(b)

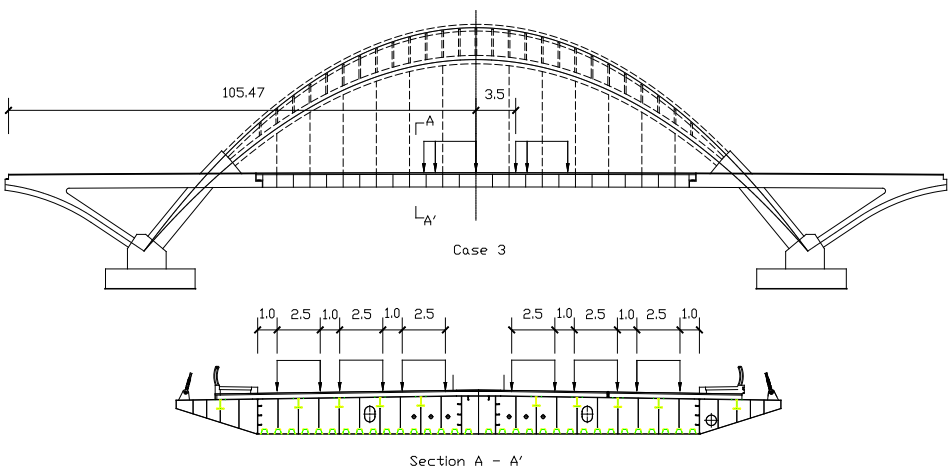

(c)

Fig. 8 Loading positions for different static load test cases and displacement measurement points (unit: m). **a** Case 1 (4 trucks in 1 row). **b** Case 2 (6 trucks in 2 rows). **c** Case 3 (12 trucks in 2 rows). **d** Case 4 (12 trucks in 2 rows). **e** Case 5 (6 trucks in 2 rows). **f** Case 6 (12 trucks in 2 rows). **g** Displacement measurement points

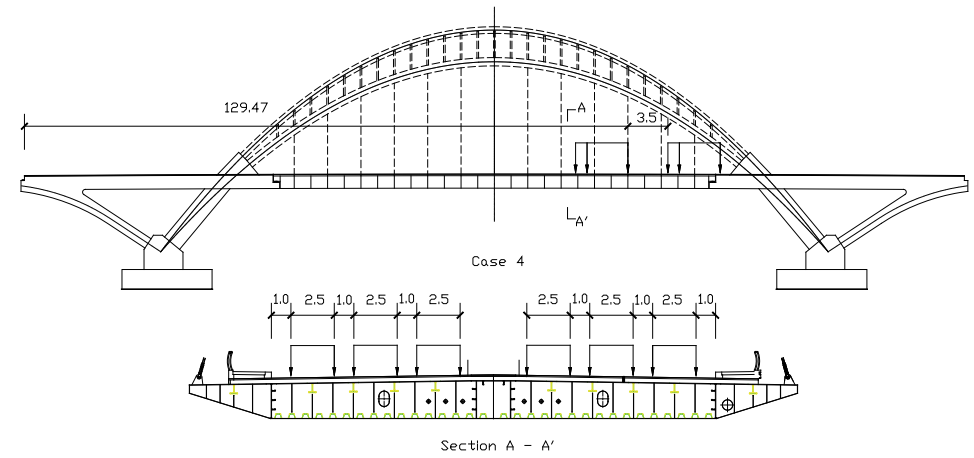

(d)

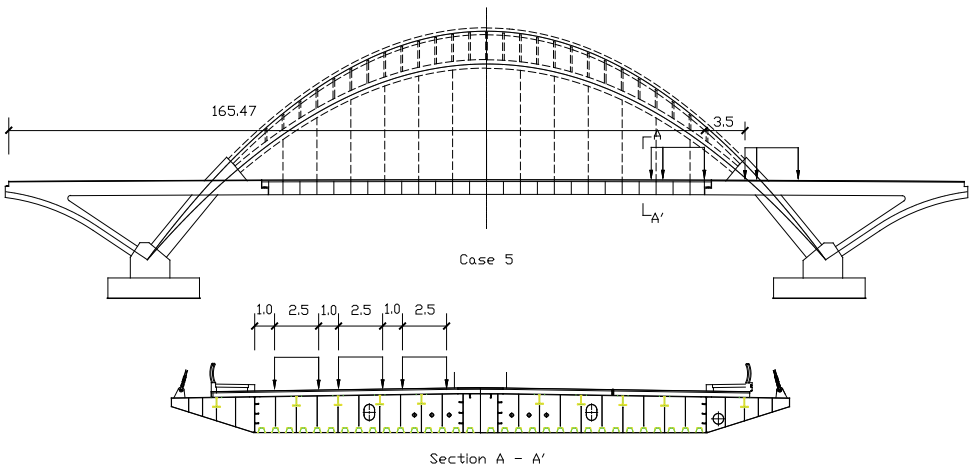

(e)

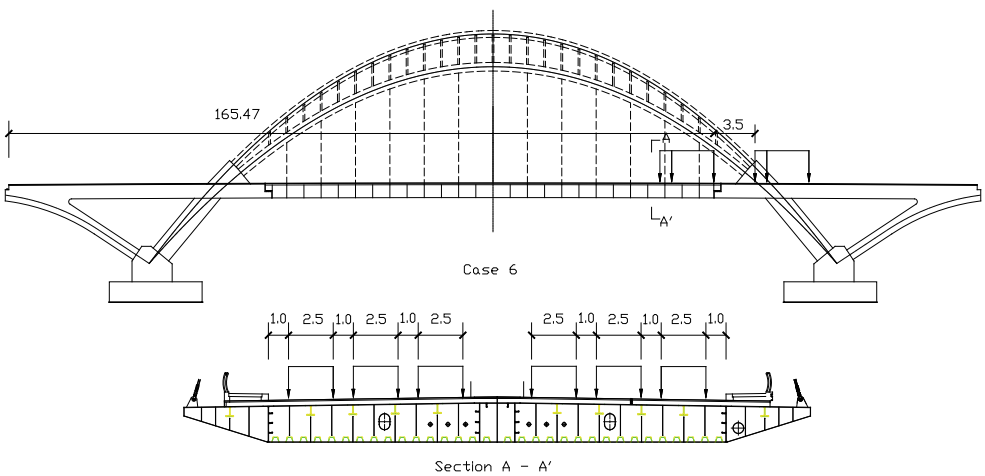

(f)

Fig. 8 continued

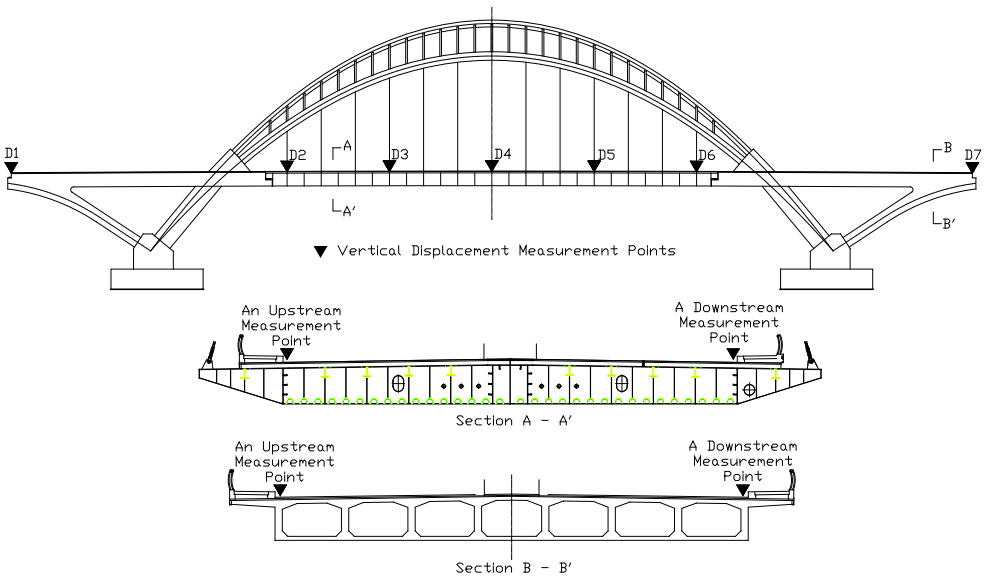

(g)

Fig. 8 continued

Table 5 Stability eigenvalues for eight load cases

	Case 1	Case 2	Case 3	Case 4	Case 5	Case 6	Case 7	Case 8
Lowest order out-plane eigenvalue	9.93	9.92	8.65	7.15	8.31	8.06	6.46	6.45
Instability shape	Out-plane antisymmetric							
Lowest order in-plane eigenvalue	32.29	–	27.94	22.96	26.84	25.96	20.67	–
Instability shape	In-plane antisymmetric							

Table 6 Strut number—stability eigenvalue

Strut number	Stability eigenvalue				
	First order	Second order	Third order	Fourth order	Sixth order
13	6.45	6.81	10.86	14.18	20.67
25	6.90	7.34	11.33	14.66	20.53

According to Table 7 and Fig. 14, after K-shaped or X-shaped struts are added to the original design, the bridge out-plane stability has improved significantly. The averaged low-order (first four lowest orders) eigenvalue increases are 24.5, 67, 73.7 and 61.2% for Cases 1–4, respectively. This indicates that adding K-shaped struts near 1/4 midspans (Cases 2–4) is an effective way to improve the structure's lateral stability.

Moreover, when K-shaped or X-shaped struts are added, the bridge's instability shape has changed notably. Except Case 3, the first order instability shapes are no longer the antisymmetric pattern of the original design (see Fig. 15).

Table 7 Strut type–stability eigenvalue

Strut type	Stability eigenvalue				
	First order	Second order	Third order	Fourth order	Sixth order
Original design	6.45	6.81	10.86	14.18	20.67
Case 1	7.03	9.83	14.95	15.17	20.57
Case 2	11.8	12.42	17.32	20.3	20.59
Case 3	8.54	16.15	19.25	20.91	20.6
Case 4	6.8	12	22.19	22.5	20.63

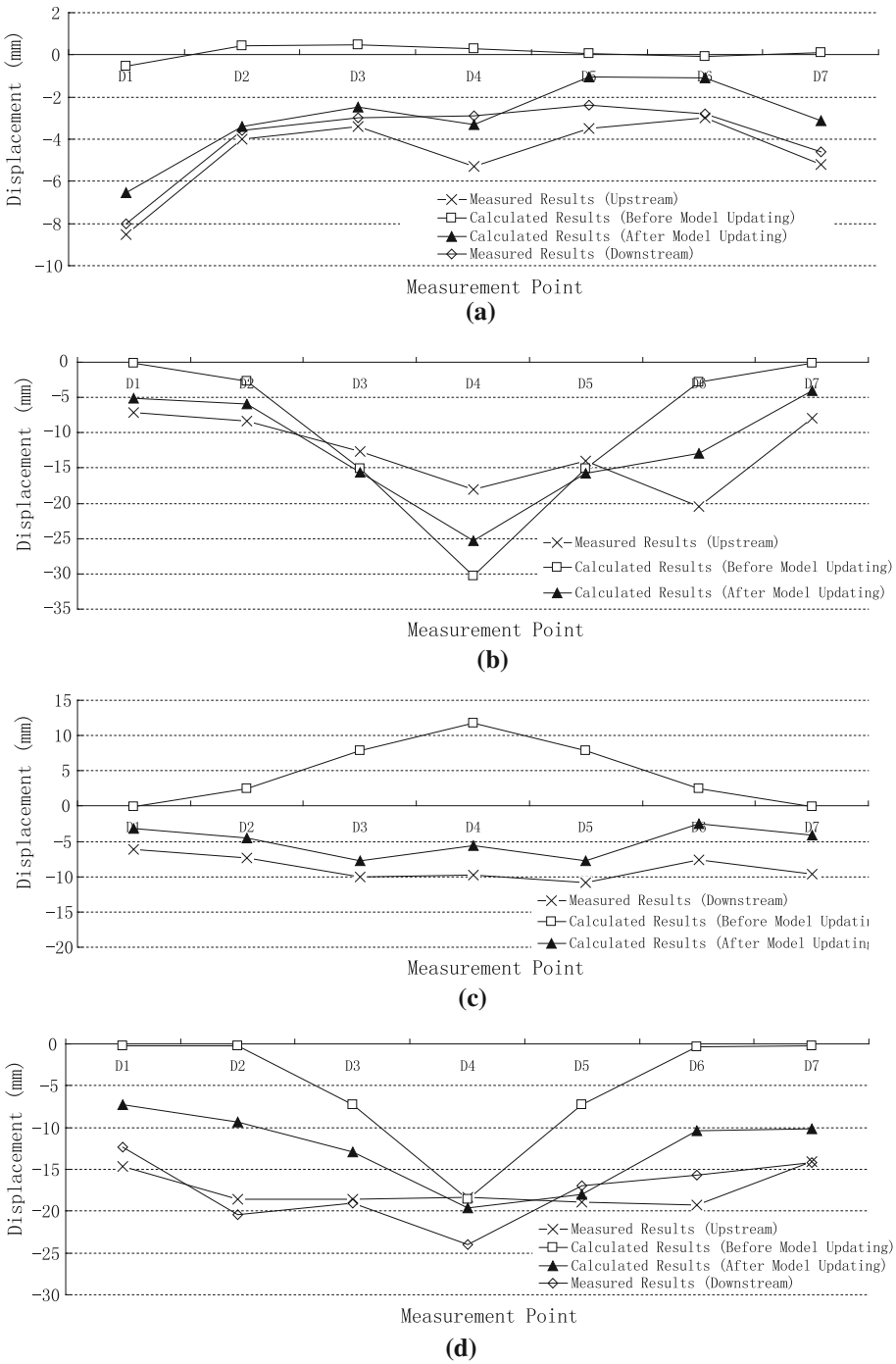

Fig. 9 Measured and calculated structural static responses. **a** Case 1. **b** Case 2 (upstream). **c** Case 2 (downstream). **d** Case 3. **e** Case 4. **f** Case 5 (upstream). **g** Case 5 (downstream). **h** Case 6

Comparing to adding horizontal struts, using K-shaped or X-shaped struts is more effective and economical. Since the first-order eigenvalue for Case 2 is larger than those of other cases, adding K-shaped struts in between midspan and 1/4 midspans is recommended.

4.1.4 Structural Stability for the Structure with Increased Stiffness of Struts

To study the effects of horizontal struts' stiffness on the structural stability, 10 cases are determined by increasing the

Fig. 9 continued

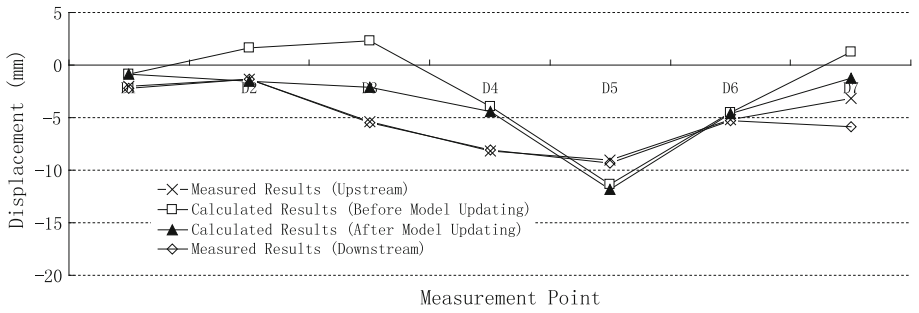

(e)

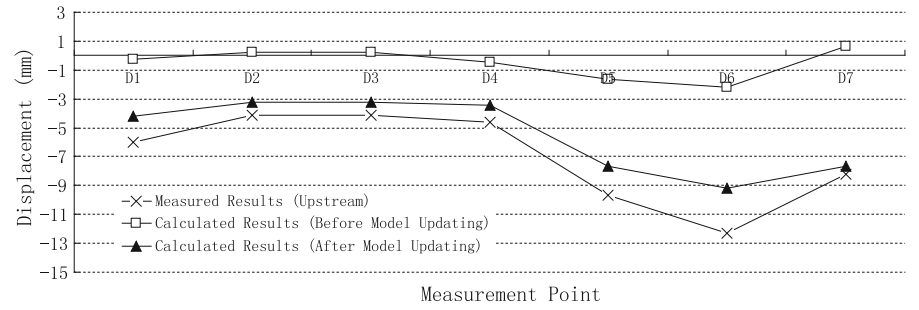

(f)

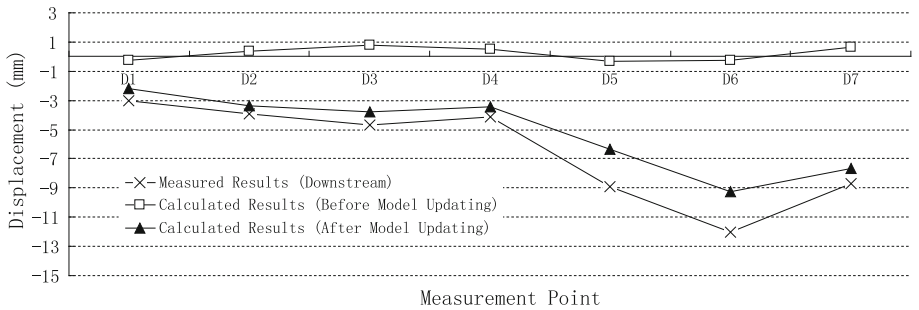

(g)

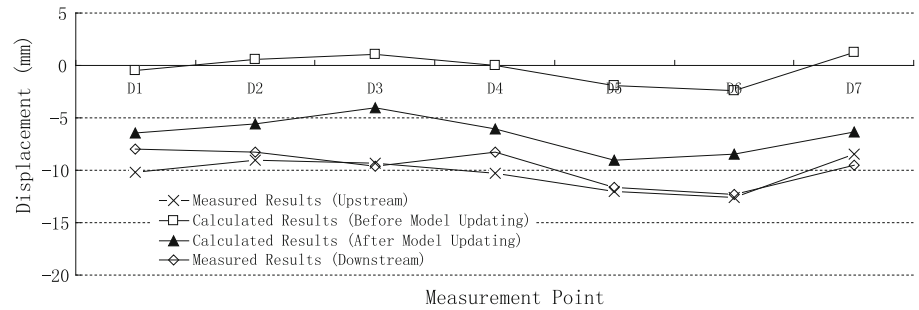

(h)

stiffness of struts from 0.2 to 2.0 times the design value. With the original strut number and strut type, the structural stability for different stiffness of struts is calculated. Results shown in Fig. 16 indicate that the effects of increased stiffness of struts are insignificant on the six lowest order stability eigenvalues.

4.1.5 Structural Stability for the Structure with Changed Inclination Angle of Subarches

Using Load Case 7, the stability analyses are conducted considering different inclination angles between the main arch and the subarches. Five inclination angles are exam-

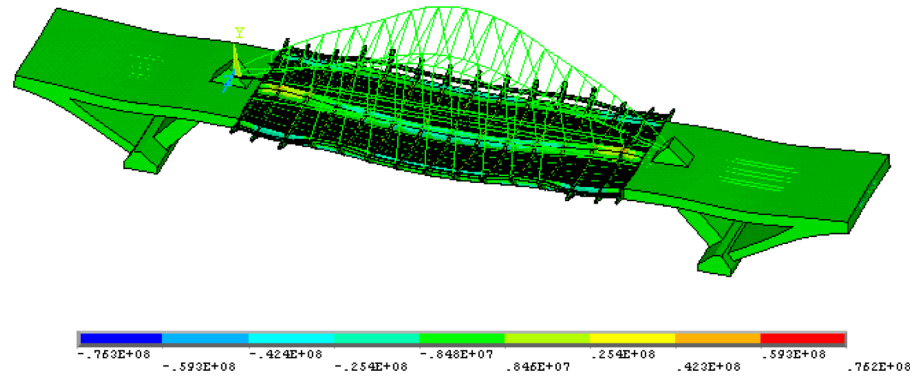

(a)

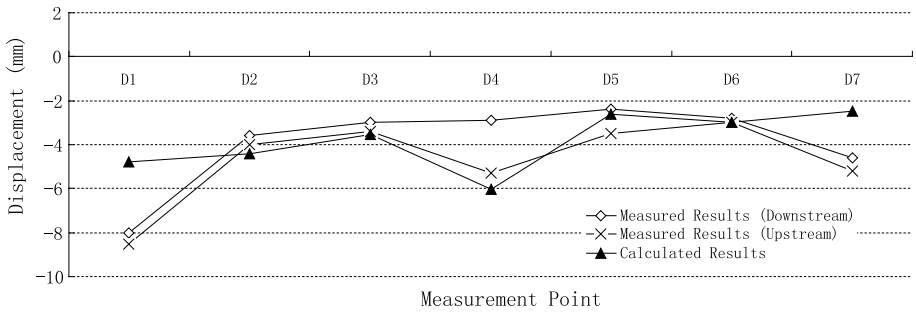

(b)

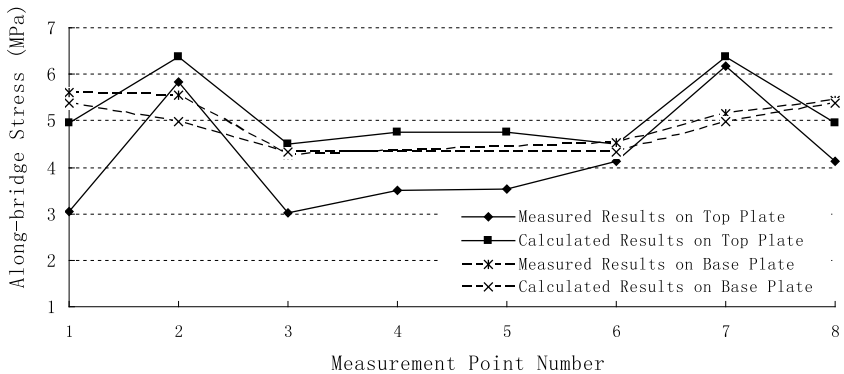

(c)

Fig. 10 Simulated results for static load test case 1 using the detailed FE model. **a** Contour plot for along-bridge stress (unit: Pa). **b** Measured and calculated displacements. **c** Measured and calculated along-bridge stresses at midspan cross section

ined, i.e., 15°, 18.75°, 21.79°, 26.25° and 30°. The results shown in Fig. 17 suggest that the obtained low-order stability eigenvalues all decrease with the increase in inclination angle within the range 15°–30°. The effect of changed inclination angle of subarches on the first-order stability eigenvalue is particularly noticeable. In this regard, a comparatively small inclination angle of subarches is suggested in designing bridges of this type.

4.1.6 Structural Stability for the Structure with Increased Stiffness of Inclined Hangers

Five cases are determined for studying the effects of increased stiffness of inclined hangers on structural stability. Results shown in Fig. 18 suggest that the effects are insignificant for out-plane (first four lowest order) structural stabilities. However, the effects for in-plane (6th order) structural stability are noticeable.

4.1.7 Structural Stability for the Structure with Increased Torsional Stiffness of the Box Girder

When lateral instability occurs for arch bridges, the hangers' positions may change, inducing additional horizontal forces on arches. For through-arch bridges, the additional horizontal forces may help arches to resist instability [15]. As hangers are attached to the box girder, the helpful effects

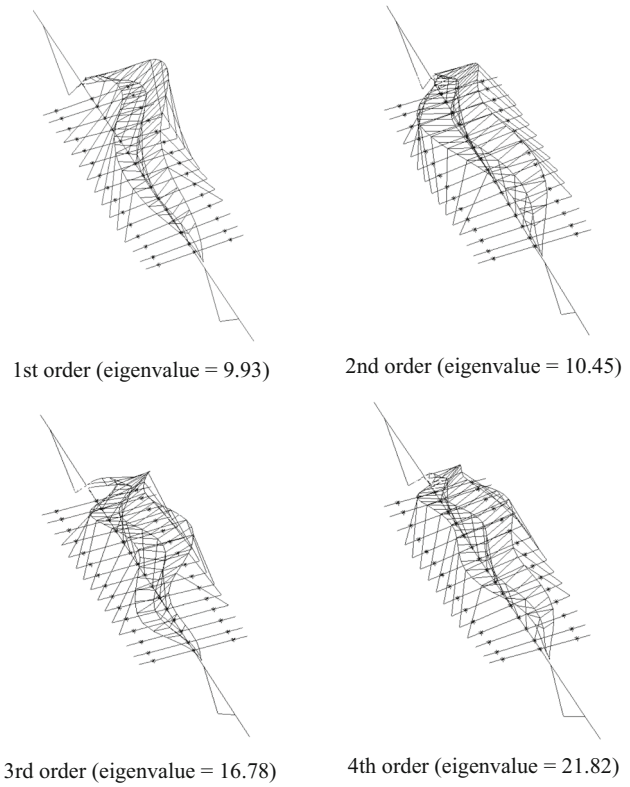

Fig. 11 Low-order instability shapes for Load Case 1

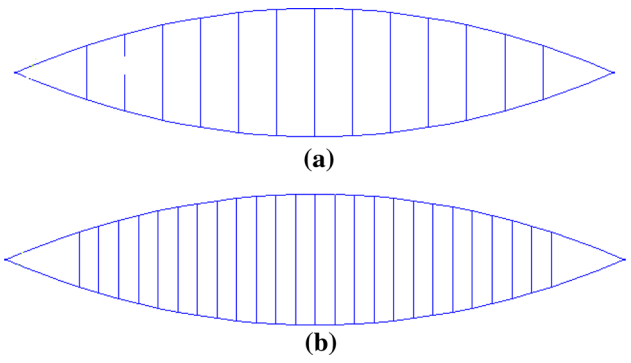

Fig. 12 Different number of struts. **a** 13 struts. **b** 25 struts

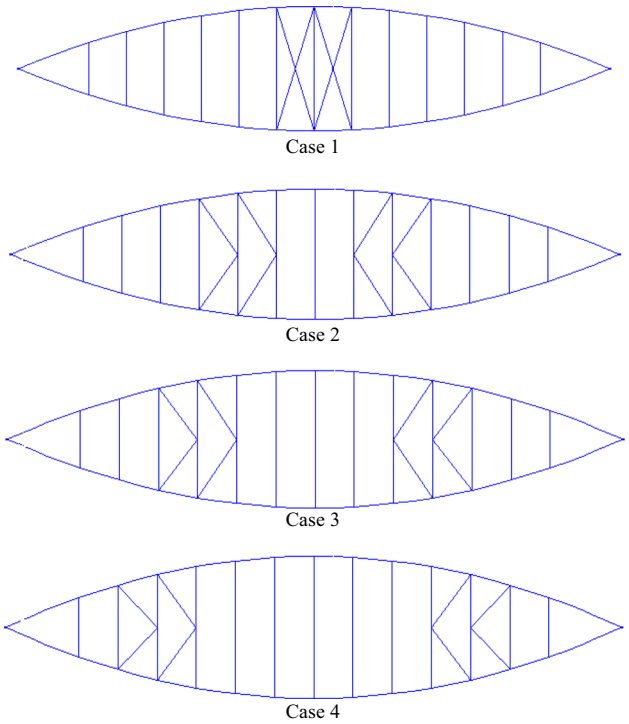

Fig. 13 Different types of struts. **a** Case 1, **b** Case 2, **c** Case 3, **d** Case 4

directly depend on the box girder's torsional stiffness. In this regard, the effects of increased torsional stiffness of the box girder on structural stability are studied in this portion of the study. The stability analyses are conducted for 5 cases. The results shown in Fig. 19 indicate that the effects are insignificant. Besides, increasing torsional stiffness of the box girder can only be realized by adjusting diaphragms in the box girder, which are comparatively difficult to implement. So, this countermeasure is not recommended.

4.2 Ultimate Load-Carrying Capacity

Ultimate load-carrying capacity analysis is based on the concept of ultimate design. According to the concept of ultimate design, the yielding of some components does not represent the failure of the whole structure. Structures can stand loads much greater than those causing the initial yielding of some components, and the marginal strength should be taken into account in design. For the ultimate load-carrying capacity analysis, the static loads are applied in a linearly step-by-step increasing manner taking into account both material and geometric nonlinear effects. With the increase in static loads, a few components begin to yield first. But the loads continue to apply, and more components are gradually found to be damaged. This process might be accompanied by obvious structural deformations. Finally, the whole structure reaches

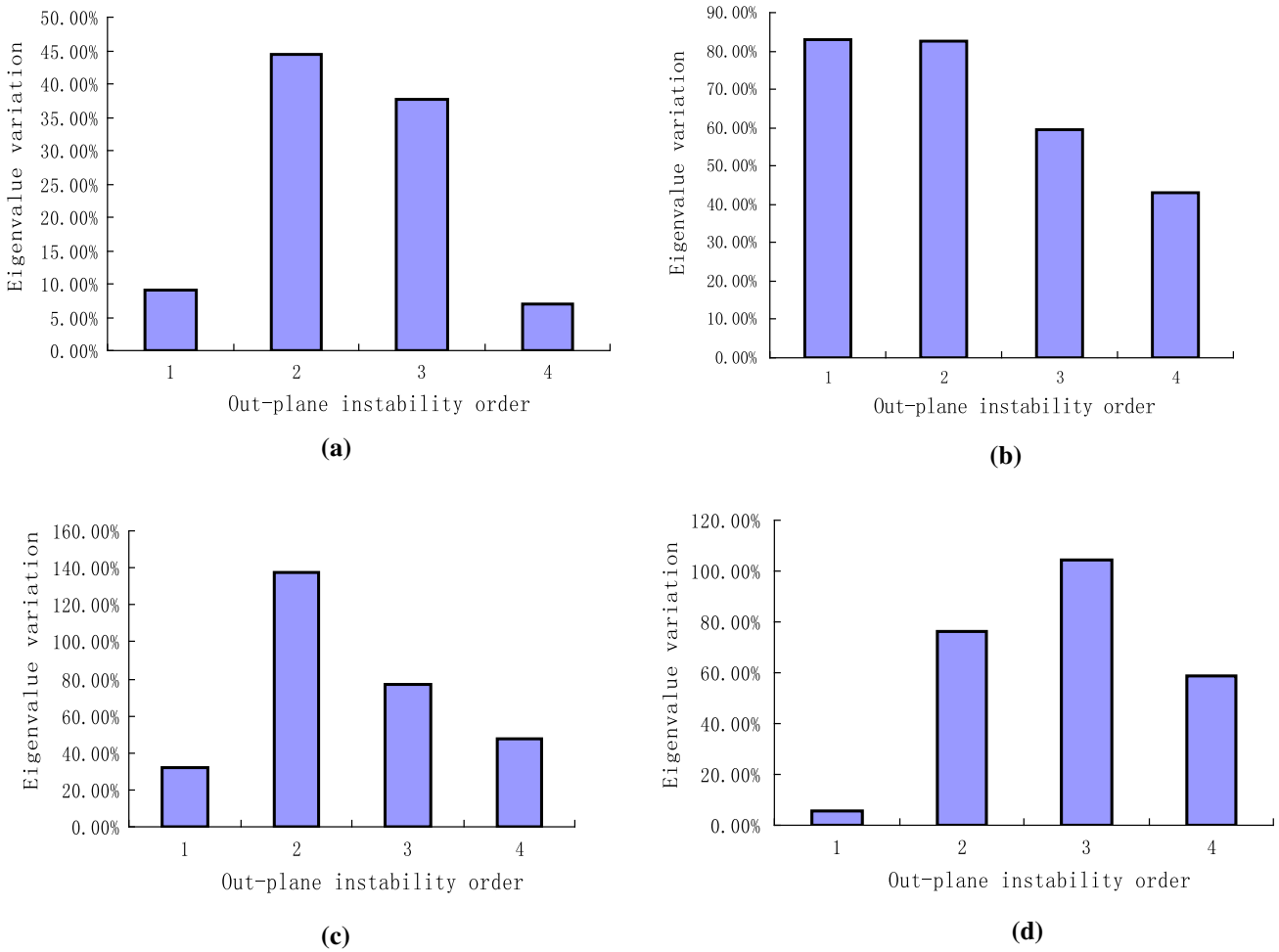

Fig. 14 Eigenvalue increases after adding different types of struts. **a** Case 1, **b** Case 2, **c** Case 3, **d** Case 4

its ultimate state, which is suggested by the occurrence of the numerical computation's failure to converge.

4.2.1 Ultimate Load-Carrying Capacity for Different Loading Modes

Two loading modes are used for calculating the ultimate load-carrying capacity of Yingzhou Bridge. For Loading Mode A, the dead load and the wind load are kept unchanged throughout the loading process, and the live loads (the lane load and the pedestrian load) are increased in a step-by-step manner until the structure fails. For Loading Mode B, the dead load is kept unchanged, but the wind load and the live loads are increased.

Through numerical analyses, the load-displacement curves are obtained at both the vault of the main arch and the midspan of the box girder, and they are shown in Figs. 20 and 21 for Loading Mode A and Loading Mode B, respectively. In Fig. 20, the curves for both the vertical displacement at the vault of the main arch and that at the midspan of the box girder show some obvious elastic-plastic features. Taking the curve of the vertical displacement at the vault of the main arch as an example, two turning points can be found at 5.0 * Pd and 5.4 * Pd (Pd is the design load), separating the whole loading process into three stages. During the first stage (0–5.0*Pd), the load is proportional to the displacement, so the structure is in elastic state and no component yields. During the second stage (5.0*Pd–5.4*Pd), the displacement increases fast, and the load is no longer in direct proportion to the displacement. Some components yield, and stiffness of the whole structure has been reduced. During the third stage (5.4*Pd–5.8*Pd), with limited increase of the load, severe structural deformation occurs. The maximum vertical displacement exceeds 0.3 m at 5.8*Pd. For a concrete-filled steel tubular arch, the plastic feature is very obvious. Based on the above, 5.4*Pd can be regarded as the yielding strength of the whole structure, and 5.8*Pd is the ultimate load-carrying capacity, where the numerical computation fails to converge. Also from Fig. 20, the vertical displacement at midspan of the box girder is greater than

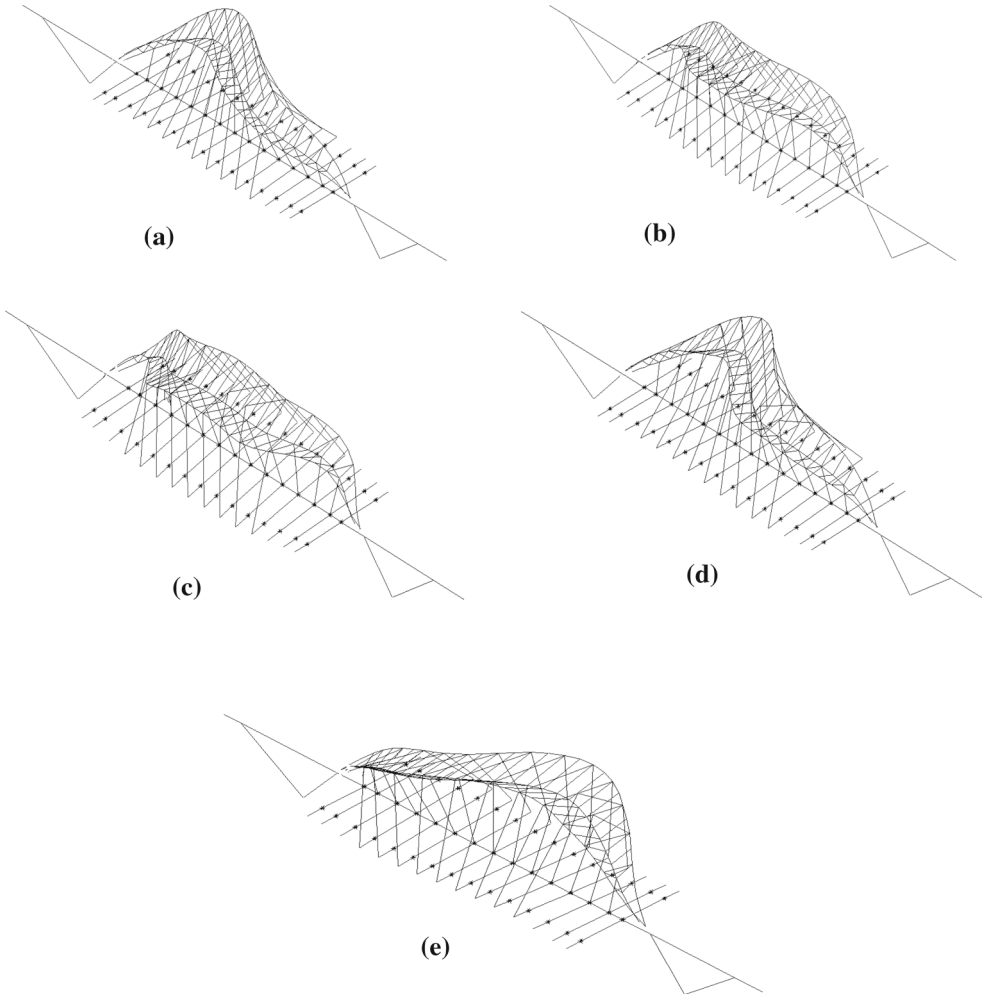

Fig. 15 First-order instability shape for the bridge with new types of struts. **a** Original design, **b** Case 1, **c** Case 2, **d** Case 3, **e** Case 4

that at the vault of the main arch after 2.0*Pd, and similar elastic–plastic features are shown for the curve of the vertical displacement at midspan of the box girder. At the ultimate state (5.8*Pd), the vertical displacement at midspan of the box girder is excessive.

Beside the vertical live load, Loading Mode B amplifies the lateral wind load. So the analyses based on Loading Mode B can demonstrate the spatial elastic–plastic features of the structure. It can be seen from Fig. 21 that the yielding strength and the ultimate load-carrying capacity of the structure are 5.1*Pd and 5.6*Pd, respectively. At the ultimate state (5.6*Pd), the structure shows a notable lateral instability shape. The lateral displacement at the vault of the main arch reaches 0.49 m at 5.6*Pd, which is much greater than the structure's in-plane displacement. In this regard, ultimate load-carrying capacity analysis equally reveals the structure's poor lateral stability.

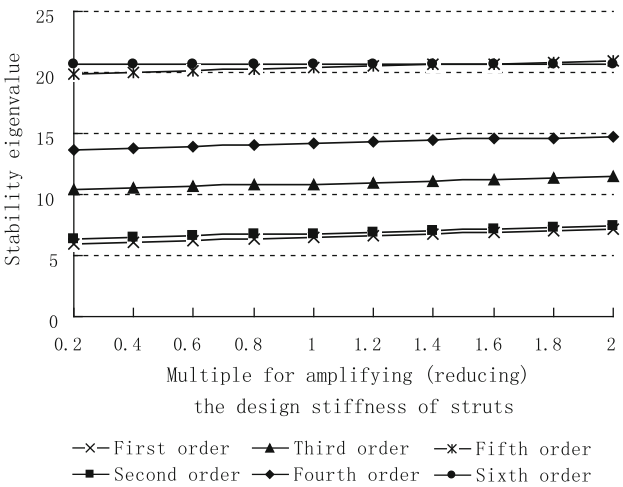

Fig. 16 Effects of stiffness of struts on stability eigenvalue

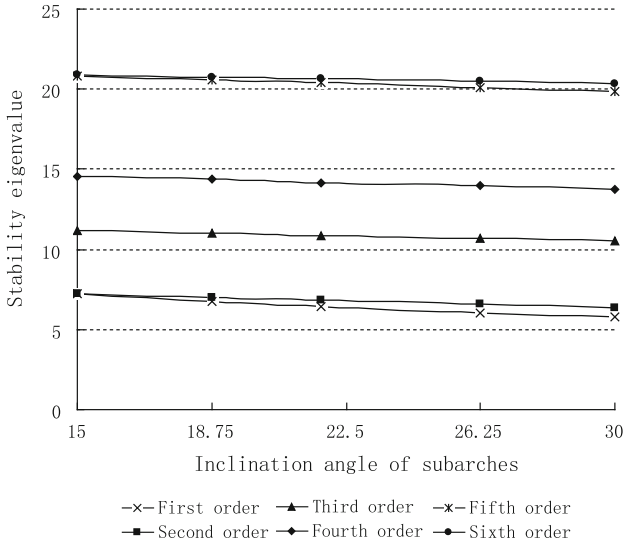

Fig. 17 Effects of inclination angle of subarches on stability eigenvalue

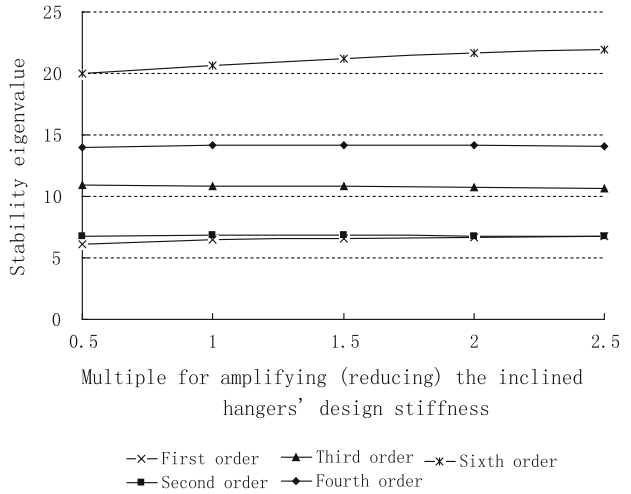

Fig. 18 Effects of stiffness of inclined hangers on stability eigenvalue

4.2.2 *Ultimate Load-Carrying Capacity for Yingzhou Bridge with K-Shaped Struts*

According to Sect. 4.1.3, adding K-shaped struts in between midspan and 1/4 midspan is the most effective countermeasure for improving the bridge's linear elastic structural stability. In this portion of study, the ultimate load-carrying capacity for the modified structure with K-shaped struts in between midspan and 1/4 midspans (Case 2 in Sect. 4.1.3) is compared with that for the original design to further verify the effectiveness of the helpful countermeasure.

Utilizing Loading Mode B, the analyses are conducted for the structure with and without K-shaped struts. According to Fig. 22, the countermeasure has no influence on the ultimate load-carrying capacity, but the structure's lateral displacement has been effectively reduced by adding K-shaped struts. At the ultimate state, the lateral displacement at the vault of the main arch reduces by around 10% by adding the K-shaped struts. In this regard, it has been proved again that adding a few K-shaped struts can effectively improve the bridge's lateral stability.

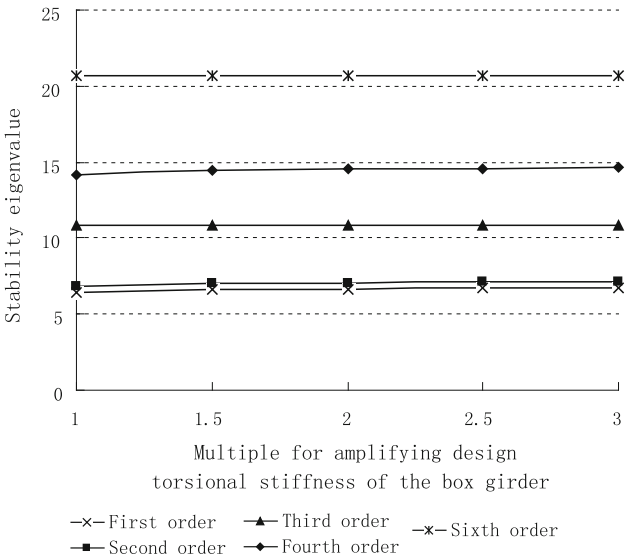

Fig. 19 Effects of torsional stiffness of the box girder on stability eigenvalue

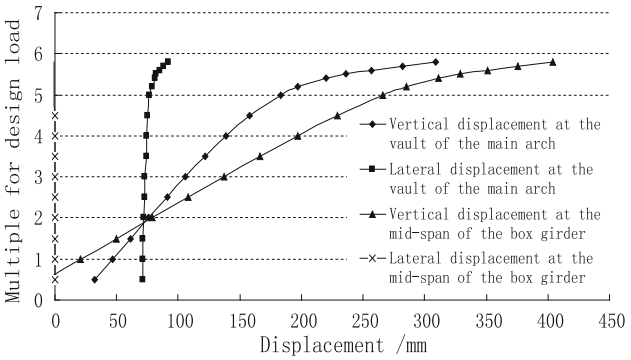

Fig. 20 Load-displacement curves for Loading Mode A

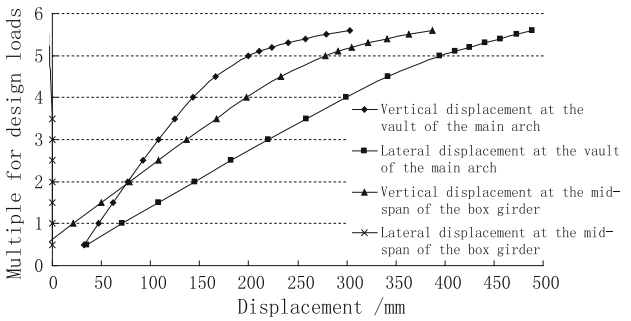

Fig. 21 Load-displacement curves for Loading Mode B

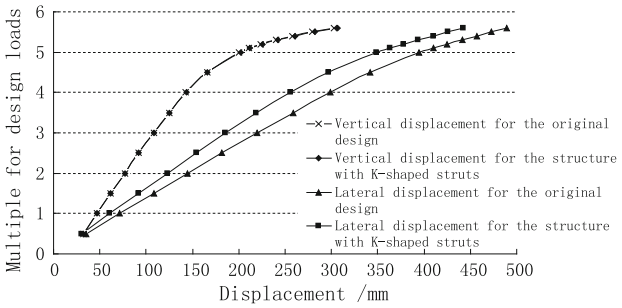

Fig. 22 Load-displacement curves obtained at the vault of the main arch for Yingzhou Bridge with/without K-shaped struts

5 Seismic Performance

Since the seismic performance is engineers' major concern in designing large arch bridges [18–25], this portion of study calculates Yingzhou Bridge's seismic performances with and without K-shaped struts in between midspan and 1/4 midspans. Nonlinear transient analyses are performed using the acceleration time-histories of the three-dimensional ground motion in Tianjin earthquake (see Ref. [26]). A representative 5-s horizontal acceleration time-history shown in Fig. 23 is considered, in which the peak ground acceleration can be found at 3.8 s. The Newmark method is used to solve the dynamic equilibrium equation for each load step.

The lateral displacements of the whole bridge with and without K-shaped struts at 3.8 s are shown in Fig. 24. According to Fig. 24, the maximum and the minimum lateral displacements are at the vault and the foot of the arch-rib system, respectively. Comparing Fig. 24a, b, it can be found that the lateral displacements are reduced significantly after K-shaped struts are added to the structure. The axial direct stresses of the whole bridge with and without K-shaped struts at 3.8 s are shown in Fig. 25. It can be found that although the maximum values are found at the foot of the arch-rib system for both structural forms, the distributions of stresses are quite different. After K-shaped struts are added to the structure, the maximum axial direct stresses are greatly reduced.

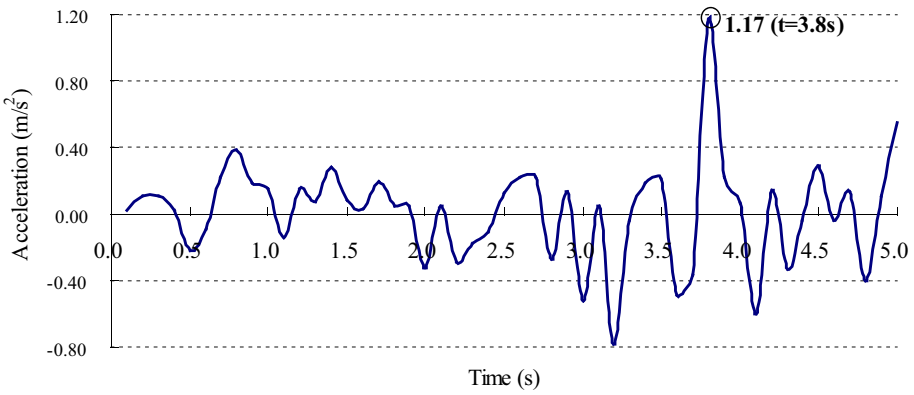

Fig. 23 Acceleration time-history of the horizontal ground motion in Tianjin earthquake

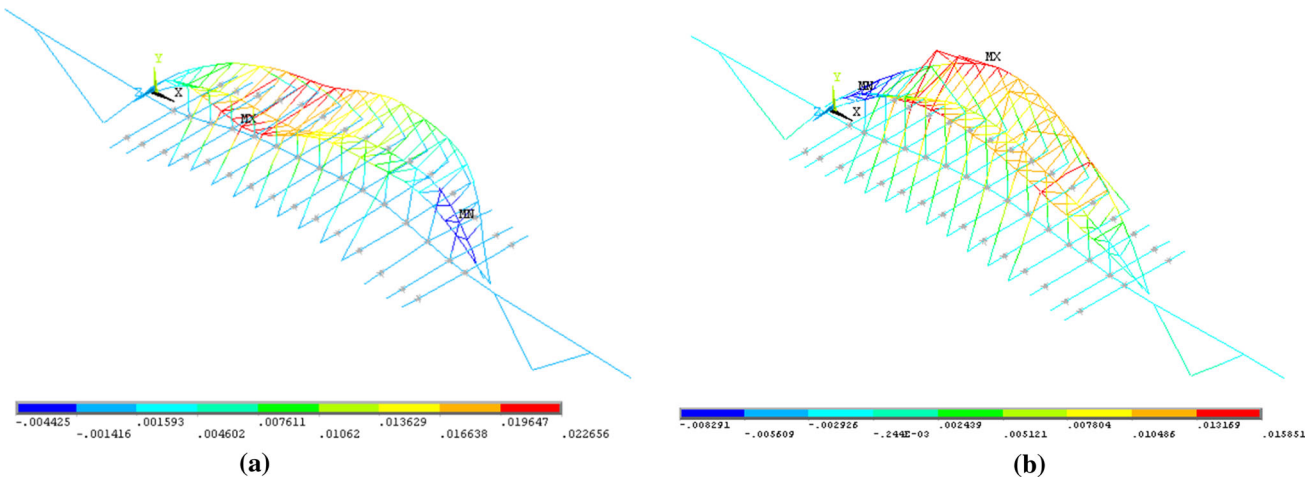

Fig. 24 Contours of lateral displacement for the whole bridge with (**b**) and without (**a**) K-shaped struts at 3.8 s (unit: m)

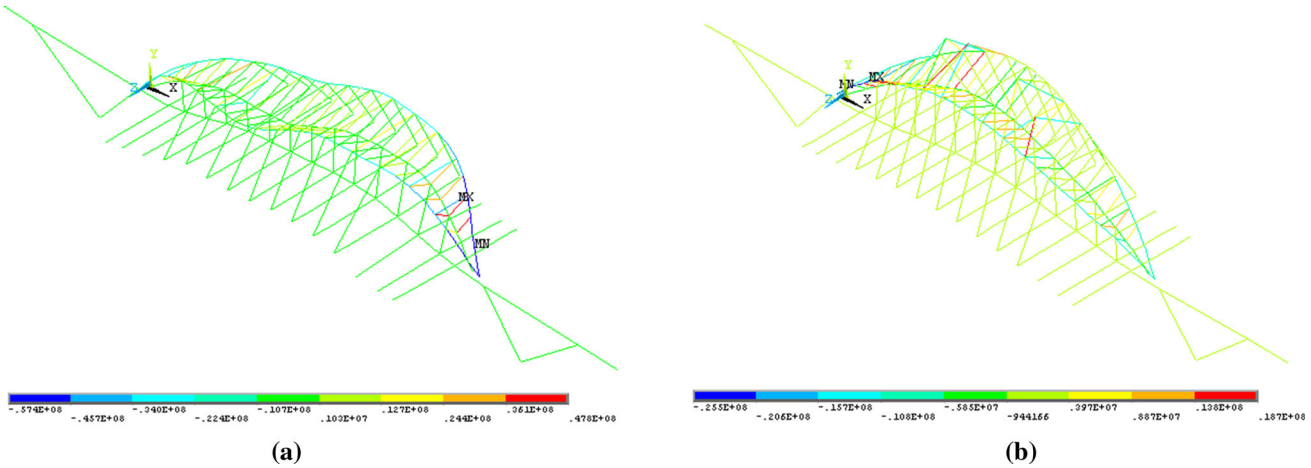

(a) (b)

Fig. 25 Contours of axial stress for the whole bridge with (**b**) and without (**a**) K-shaped struts at 3.8 s (unit: Pa)

6 Conclusion

For large civil engineering structures, ambient modal tests might produce uncertain results due to many influences, e.g., the measurement noise, the effects of modal identification method and the temperature variation. To acquire reliable reference information for model updating, detailed models can be employed, whose spatial distributions of mass and stiffness are highly accurate. In this paper, Yingzhou Bridge's simplified computational model is updated following this practice. After model updating, the static structural responses obtained using the computational model agree well with those measured on the real structure, which suggests that a satisfactory computational model is established.

Using the validated computational model, Yingzhou Bridge's structural stability, ultimate load-carrying capacity and seismic performance are calculated. Results suggest that the innovative structure's static and dynamic behaviors both meet the design requirements. However, according to structural stability analyses, the five lowest order instability shapes are out-plane patterns for all the eight load cases. Besides, ultimate load-carrying capacity analyses and seismic performance analyses both suggest that the bridge's lateral structural responses are comparatively large when experiencing extreme events. These observations all indicate that Yingzhou Bridge's lateral stability and stiffness are relatively weak. This problem should be mitigated to prevent the structural failure in the following scenarios: (1) Slight lateral disturbances occur when the bridge is overloaded; (2) live loads (the lane load and the pedestrian load) on the bridge are crosswise eccentric; (3) earthquake excitations and wind loads act on the bridge laterally.

To enhance the bridge's lateral stability and stiffness, six usual countermeasures are proposed and individually examined in this paper. It is found that adding K-shaped struts between subarches and reducing subarches' angle of inclination can effectively increase the bridge's lateral stability eigenvalues, and after K-shaped struts are added between the subarches, the bridge's lateral structural responses under the excessive loading and the earthquake are greatly reduced. Thus, adding K-shaped struts between subarches and reducing subarches' angle of inclination are two effective approaches to enhance the bridge's lateral stability and stiffness. For a bridge open to traffic, adding K-shaped struts is practicable, but reducing the subarches' angle of inclination cannot be realized. For future design practices for this type of bridge, both of the two approaches are of practical significance.

References

1. Li, Y.; Cai, C.S.; Liu, Y.; Chen, Y.; Liu, J.: Dynamic analysis of a large span specially shaped hybrid girder bridge with concrete-filled steel tube arches. Eng. Struct. **106**, 243–260 (2016)
2. Zhang, D.-Y.; Li, X.; Yan, W.-M.; Xie, W.-C.; Pandey, M.D.: Stochastic seismic analysis of a concrete-filled steel tubular (CFST) arch bridge under tridirectional multiple excitations. Eng. Struct. **52**, 355–371 (2013)
3. Fei, Q.G.; Li, A.Q.; Han, X.L.; Miao, C.Q.: Modal identification of long-span Runyang Bridge using ambient responses recorded by SHMS. Sci. China Ser. E Technol. Sci. **52**, 3632–3639 (2009)
4. Bayraktar, A.; Birinci, F.; Altunisik, A.C.; Turker, T.; Sevim, B.: Finite element model updating of Senyuva historical arch bridge using ambient vibration tests. Balt. J. Road Bridge Eng. **4**, 177–185 (2009)
5. Bayraktar, A.; Sevim, B.; Altunisik, A.C.; Turker, T.: Earthquake analysis of reinforced concrete minarets using ambient vibration test results. Struct. Des. Tall Special Build. **19**, 257–273 (2010)
6. Abdel Wahab, M.; De Roeck, G.: Effect of temperature on dynamic system parameters of a highway bridge. Struct. Eng. Int. **7**, 266–270 (1997)
7. Cornwell, P.; Farrar, C.R.; Doebling, S.W.; Shoh, H.: Environmental variability of modal properties. Exp. Tech. **23**, 45–48 (1999)
8. Ding, Y.L.; Li, A.Q.: Temperature-induced variations of measured modal frequencies of steel box girder of a long-span suspension bridge. Int. J. Steel Struct. **11**, 145–155 (2011)

9. Teng, J.; Zhu, Y.; Zhou, F.; Li, H.; Ou, J.: Finite element model updating for large span spatial steel structure considering uncertainties. J. Cent. South Univ. Technol. **17**, 857–862 (2010)
10. Brownjohn, J.M.W.; Xia, P.-Q.: Dynamic assessment of curved cable-stayed bridge by model updating. J. Struct. Eng. ASCE **126**(2), 252–260 (2000)
11. Kilic, S.A.; Raatschen, H.J.; Körfgen, B.; Apaydin, N.M.; Astaneh-Asl, A.: FE model of the Fatih Sultan Mehmet Suspension Bridge using thin shell finite elements. Arab. J. Sci. Eng. (2016). doi:10.1007/s13369-016-2316-y
12. Jaishi, B.; Ren, W.-X.: Structural finite element model updating using ambient vibration test results. J. Struct. Eng. ASCE **131**(4), 617–628 (2005)
13. Wu, Y.: Load test of special-shaped concrete-filled steel-tube arch bridge and analysis of unitary stability. MSc Dissertation, Southeast University, Nanjing, China (in Chinese) (2010)
14. Ministry of Transport, P.R.C.: JTG D60-2004: General Code for Design of Highway Bridges and Culverts (in Chinese) (2004)
15. Xiang, H.F.: Advanced Theories for Bridge Structures. China Communications Press, Beijing (2001). (in Chinese)
16. Sun, Z.S.; Yan, F.; Fan, K.J.: Analyses on dynamic characteristics of a special-shaped half-through concrete-filled steel tubular arch bridge. J. Highw. Transp. Res. Dev. (Appl. Technol. Ed.) **7**, 22–24 (2008). (in Chinese)
17. Hua, X.G.; Ni, Y.Q.; Chen, Z.Q.; He, X.H.: Monte Carlo study of the effect of measurement noise in model updating with regularization. J. Eng. Mech. ASCE **138**(1), 71–81 (2012)
18. Khan, E.; Sullivan, T.J.; Kowalsky, M.J.: Direct displacement-based seismic design of reinforced concrete arch bridges. J. Bridge Eng. ASCE **19**(1), 44–58 (2014)
19. Torkamani, M.A.M.; Lee, H.E.: Dynamic behavior of steel deck tension-tied arch bridges to seismic excitation. J. Bridge Eng. ASCE **7**(1), 57–67 (2002)
20. Nonaka, T.; Ali, A.: Dynamic response of half-through steel arch bridge using fiber model. J. Bridge Eng. ASCE **6**(6), 482–488 (2001)
21. Wu, Q.; Yoshimura, M.; Takahashi, K.; Nakamura, S.; Nakamura, T.: Nonlinear seismic properties of the Second Saikai BridgeA concrete filled tubular (CFT) arch bridge. Eng. Struct. **28**, 163–182 (2006)
22. Zanardo, G.; Pellegrino, C.; Bobisut, C.; Modena, C.: Performance evaluation of short span reinforced concrete arch bridges. J. Bridge Eng. ASCE **9**(5), 424–434 (2004)
23. Liu, C.; Wang, Y.; Wang, W.; Wu, X.: Seismic performance and collapse prevention of concrete-filled thin-walled steel tubular arches. Thin-Walled Struct. **80**, 91–102 (2014)
24. Wen, R.K.: Seismic response of and design aids for arch bridges. J. Struct. Eng. ASCE **119**(10), 2969–2985 (1993)
25. Tang, Z.; Xie, X.; Wang, T.; Wang, J.: Study on FE models in elasto-plastic seismic performance evaluation of steel arch bridge. J. Construct. Steel Res. **113**, 209–220 (2015)
26. Hao, W.H.: Applications of ANSYS in Civil Engineering. China water and power press, Beijing (2005). (in Chinese)
27. ANSYS, Inc.: ANSYS Release 9.0 Documentation. (2004)